ADVANCED HEALTHCARE MATERIALS
www.advhealthmat.de

Flexible Short Silica Fibers and Tricalcium Phosphate Synergistically Promote Bone Fracture Healing in Composite Cryogel Scaffolds

Xinyi Wang, Zhengchao Yuan, Guangfang Cai, Yifan Lu, Shasha Zhou, Panpan Shang, Cheng Li, Zewen Wang, Zhenchao Liu, Muhammad Shafiq, Mohamed EL-Newehy, Meera Moydeen Abdulhameed, Xiao Lu, Yuan Xu,* and Xiumei Mo**

Bone tissue engineering is a critical area of research focused on enhancing the regeneration of bone tissue, particularly in cases of complex defects. Despite inherent self-healing capabilities of bone, irregularly-shaped defects pose significant challenges for complete regeneration, thereby necessitating innovative therapeutic strategies. This study addresses these challenges by exploring the development of advanced tissue regeneration scaffolds. Here, tricalcium phosphate (TCP) is integrated with short silica (SiO_2) fibers to develop 3D cryogel scaffolds, designated as SSFx@TCP. These cryogel scaffolds exhibit low density (<2 mg cm^{-3}), high water absorption (>3500%), and favorable sustained release properties, enabling effective cellular interactions. Notably, the SSFx@TCP cryogels support cell attachment, proliferation, and differentiation, while also regulate gene expression associated with angiogenesis and osteogenesis. Furthermore, in vivo assays demonstrated that these scaffolds can effectively promote *de novo* bone production in a rat calvarial defect model 8 weeks post-operatively, thereby indicating their potential to mimic the natural extracellular matrix. The successful integration of bioactive components in these cryogels may be beneficial for improved clinical outcomes in bone regeneration therapies and ultimately enhancing patient care in reconstructive surgery.

1. Introduction

Fracture defects due to aging, trauma, or an injury adversely affect the quality-of-life (QOL) of patients and pose a debilitating burden on the healthcare sector and an overall well-being of the mankind. Critical bone defects are difficult to be healed spontaneously, which may be due to congenital malformations, severe trauma, and malignant bone tumors. General guidelines about critical bone defects include defects with the length more than 1–2 cm and loss of more than 50% of the bone circumference.[1,2] While bone exhibits an intrinsic ability to heal smaller wounds of non-critical size, critical-sized bone defects are difficult to be healed due in part to the restricted regenerative capacity of bone tissue. The issue of poor healing in critical-sized bone defects may be further exaggerated by diseases, such as diabetes, osteoporosis, and osteosarcoma. Annually, 2.2 million bone implants are used worldwide with 500,000 in China alone, which

X. Wang, Z. Yuan, G. Cai, Y. Lu, S. Zhou, X. Mo
State Key Laboratory for Modification of Chemical Fibers and Polymer Materials
Shanghai Engineering Research Center of Nano-Biomaterials and Regenerative Medicine
College of Biological Science and Medical Engineering
Donghua University
Shanghai 201620, P. R. China
E-mail: xmm@dhu.edu.cn

P. Shang, X. Mo
Institute of Biomaterials and Biomedicine
School of Food and Pharmacy
Shanghai Zhongqiao Vocational and Technical University
Shanghai 201514, P. R. China

C. Li, Z. Wang, Y. Xu
Department of Orthopaedics
Xinqiao Hospital
Army Medical University
No.183, Xinqiao Street, Shapingba District, Chongqing 400037, P. R. China
E-mail: xuyuan88@tmmu.edu.cn

Z. Liu
Basic Medical College of Army Medical University
No.30, Gaotanyan Street, Shapingba District, Chongqing 400037, P. R. China

M. Shafiq
Innovation Center of NanoMedicine (iCONM)
Kawasaki Institute of Industrial Promotion
Kawasaki-ku, Kawasaki 210–0821, Japan

M. EL-Newehy, M. M. Abdulhameed
Department of Chemistry
College of Science
King Saud University
P.O. Box 2455, Riyadh 11451, Saudi Arabia

The ORCID identification number(s) for the author(s) of this article can be found under https://doi.org/10.1002/adhm.202404329

DOI: 10.1002/adhm.202404329

constitutes an economy of approximately $2.93 billion for the treatment of fracture repair. By keeping in view the composition of the native bone, both organic and inorganic components are required alongside mimicking hierarchical architecture of bone tissue, a blood vessel network for the diffusion of oxygen and the transport of nutrients, and the capability of osteogenesis, angiogenesis, and innervation. In addition to structural and morphological cues, biological cues, including different cell types (e.g., osteoblasts, endothelial cells, stromal cells, etc.), angiogenic and osteogenic growth factors, and therapeutic ions are often incorporated into artificial scaffold materials to induce bone tissue repair. Zhang et al. utilized digital laser processing (DLP)-based three-dimensional (3D) printing to fabricate bioceramic scaffolds that mimicked the structure of Haversian bone. These scaffolds were further integrated with a multicellular delivery platform, facilitating vascularized bone regeneration.[3] Similarly, Zhou et al. developed biomimetic scaffolds incorporating strontium-doped hydroxyapatite (SrHA) and mesoporous silica nanoparticles (DMSNs) loaded with dimethyloxalylglycine (DMOG) using a combination of 3D printing and electrospinning techniques. These scaffolds enabled the controlled release of DMOG and strontium ions (Sr^{2+}), simultaneously enhancing osteogenesis and angiogenesis.[4] Besides various commonly used inorganic nanoparticles (NPs), such as hydroxyapatite (HAp) and tricalcium phosphate (TCP) have garnered considerable attention from clinicians and surgeons due to numerous merits, including structural similarity to the bone, osteo-inductivity, and osteo-conductivity. Owing to the good cytocompatibility, the TCP has been shown to promote the adhesion and growth of osteocytes as well as enhance the differentiation of bone marrow mesenchymal stem cells (BM-MSCs) into osteogenic cells and promote graft-tissue integration.[5,6] Despite these advantageous merits, the clinical translation of TCP is severely constricted by its smaller pore size, fragility, brittleness, poor vasculogenic ability, and its ability to generate degradation products, especially, during direct interaction with the tissues at the fracture defect.[7,8]

Traditionally, organic or polymer-based matrices (e.g., collagen, gelatin, poly(L-lactide) (PLLA), etc.) are blended with inorganic components to create bone tissue engineering (TE) scaffolds. However, scaffolds composed entirely of inorganic components, such as inorganic fibers and nanomaterials (NMs), have been rarely explored, particularly in the context of bone tissue repair. Notably, short electrospun fibers made entirely of inorganic materials hold significant potential due to their ability to integrate seamlessly into 3D scaffolds, provide therapeutic ions to modulate cellular processes, and offer tunable composition. Silicon (Si) has been shown to promote osteoblast differentiation for fracture repair.[9,10] Short SiO_2 fibers have received considerable attention from the research community and shown to exhibit bioactivity and osseointegration behaviors.[11] These short SiO_2 fibers may additionally impart tunable mechanical properties to the scaffolds despite their poor degradation and limited ability to produce collagen.[12] Cryogel scaffolds based on silica fibers and TCP have been successfully fabricated and used for skin repair albeit with limitations of the individual components, such as lack of a porous structure as well as the fragility of the TCP and relatively sluggish degradation of silica.[13] Therefore, we hypothesized that composite cryogel scaffolds based on short silica fibers and TCP may avoid the above-mentioned limitations associated with the individual components, which may broaden their applicability for bone tissue regeneration.

Our strategy of the combined utilization of short silica fibers and TCP is expected to have several advantages: *i*) short SiO_2 fibers (SSF) can furnish silicon ions (Si^{4+}), which may promote simultaneous osteogenesis and angiogenesis by stimulating endothelial cells (ECs) and BMSCs,[13] *ii*) TCP can improve biofunctions, including angiogenesis and osteogenesis, rapid degradation, and biosorption, *iii*) TCP can release calcium ions (Ca^{2+}), which can activate platelet protein phosphorylation via protein kinase C (PKC) and initiate intrinsic and extrinsic coagulation pathways, thereby enhancing hemostatic capabilities.[14] Therefore, our prepared cryogel scaffolds can synergistically promote angiogenesis as well as osteogenesis using both Si^{4+} and Ca^{2+}, which may be promising for applications in bone defect reconstruction.

2. Experimental Section

2.1. Materials

Poly(vinyl alcohol) (PVA, degree of hydrolysis = 87–89%) and triethyl phosphate (TEP, purity, 99.5%) were obtained from Aladdin (Shanghai, China). Tetraethyl orthosilicate (TEOS, purity, 98%) was received from J&K Scientific (Beijing, China). Tricalcium phosphate (TCP, purity, 99%) was obtained from Beiaolu (Shanghai, China). Fetal bovine serum (FBS, product code C0235), Dulbecco's modified Eagle Medium (DMEM basic medium), and Penicillin-Streptomycin were purchased from Thermo Fisher Scientific (Shanghai, China). Live/dead cell assay kit (product code, 40203ES80) was obtained from Yeasen (Shanghai, China). The alkaline phosphatase assay kit (ALP, product code, P0321S) and Alizarin red staining kit (ARS, product code, C0138) was purchased from Beyotime (Shanghai, China). Anti-BMP2 rabbit primary antibody, anti-collagen type I rabbit antibody, and Alexa Fluor 488 were obtained from Servicebio (Wuhan, China).

2.2. Synthesis of Cryogel Scaffolds

TEOS and TEP were respectively used as precursors for the silicon (Si) and phosphorus (P) and were then mixed with PVA for electrospinning. PVA was dissolved in DI water to afford 10% (w/v) solution. Similarly, the PVA solution containing TEOS and TEP (TEOS: TEP, 1:1, w/w) were prepared. The solutions were stirred at room temperature (r.t.) for 12 h, PVA and precursor solutions were mixed (1:1, w/w) and stirred at 60 °C for another 6 h. The processing conditions of electrospinning (E02, Forhan Karuko Precision Measurement & Control Technology

X. Lu
Shanghai Orthopedic Biomaterial Technology Innovation Center
Shanghai Bio-lu Biomaterials Co., Ltd.
Shanghai, P. R. China
E-mail: xiao.lu@bio-lu.com

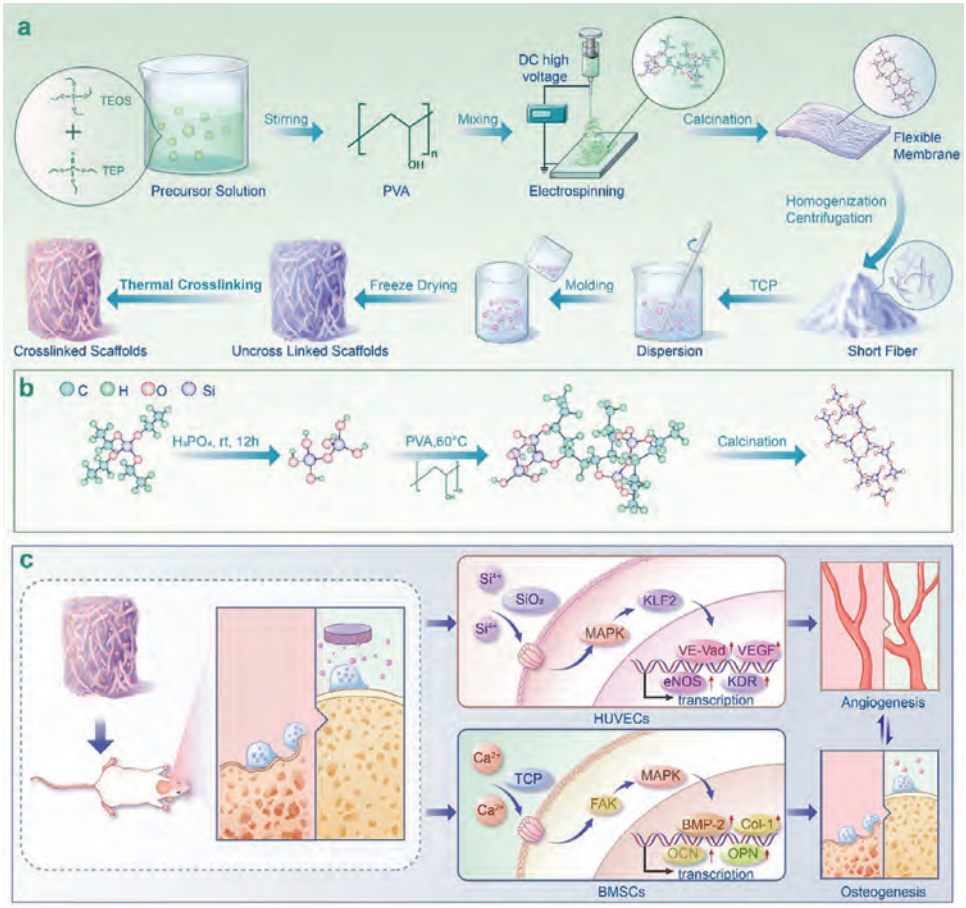

Figure 1. a) Schematic illustration for the fabrication of SSFx@TCP cryogel scaffolds. b) Preparation and molecular conformation of SiO_2 in amorphous phase. c) Mechanisms of scaffolding for bone regeneration.

Co., Ltd., China) were as follows: applied voltage, 18 kV, flow rate, 1 mL h^{-1}, rotation speed of the collector, 250 rpm, and spinneret-to-collector distance, 15 cm. As-obtained mat was dried inside a fume hood for 24 h followed by calcination in a muffle furnace (F0311C, Yamato Scientific Co., Ltd., Chongqing, China) at 800 °C for 2 h to obtain flexible silica fibers. The silica fibers were weighed and ground at 8000 rpm for 15 min using a homogenizer to obtain short silica fibers (SSF) (PD500-TP, Prima InstrumentsCo., Ltd., Shanghai, China). To prepare the cryogel solution, different contents of SSF (40, 80, and 120 mg) were dispersed in water and were then combined with the TCP. For SSF1@TCP, 40 mg of SSF was dispersed into DI water and later 40 mg TCP was added. The amount of the SSF was 80 and 120 mg, while that of the TCP was 40 mg for the SSF2@TCP and SSF3@TCP cryogel solutions, respectively. The respective cryogel solutions were then freeze-dried and thermally crosslinked. As-prepared cryogel scaffolds are shown in **Figure 1**a.

2.3. Physicochemical Characterization

Cryogel scaffolds were analyzed for physicochemical properties, including morphology, elemental analysis, the release of silicon ions (Si^{4+}) and calcium ions (Ca^{2+}), mechanical properties, density, and water absorption capacity. The detailed methods are provided in Supplementary Information.

2.4. Biocompatibility and Biological Functions of Cryogel In Vitro

For biocompatibility and biological function analysis, cryogels were evaluated for cell viability using live/dead staining, cell proliferation using CCK-8 assay, hemolysis ratio, Transwell migration assay, scratch wounding assay, biomineralization assay using Alkaline phosphatase (ALP) and Alizarin Red S (ARS) staining, and osteogenesis-related gene expressions in vitro. The detailed methods are provided in Supporting Information. HUVECs and MC3T3 used in this work were purchased from the CAS cell bank (Shanghai, China). BMSCs were isolated and cultured according to protocols established in previous studies.[15]

2.5. Animal Experiments

2.5.1. Subcutaneous Implantation of Cryogel

The osteogenesis ability of scaffolds was investigated by the subcutaneous implantation model in rats. All animal experiments

were performed in accordance with the guidelines of the Laboratory Animal Welfare and Ethics Committee of the Army Medical University (Approval # AMUWEC20237514). Briefly, SD rats (8-week-old, male, 230 ± 20 g, n = 3) were first anesthetized by using an intraperitoneal injection of 3% pentobarbital sodium (30 mg kg^{-1}). The dorsum area of each rat was shaved and sterilized with povidone-iodine, and a subcutaneous pocket was created by making an incision of ≈1 cm. The MC-3T3E1 cell suspension (10×10^5 cells) was added dropwise to the ultraviolet (UV)-sterilized scaffolds (e.g., SSF1@TCP, SSF2@TCP, SSF3@TCP, etc.), which were then quickly placed subcutaneously and sutured. After 4 and 8 weeks, scaffolds were removed and assessed for bone regenerative capacity using Micro-CT (SkyScan 1176, Bruker). The surrounding tissues were also harvested, fixed in paraformaldehyde, and then subjected to hematoxylin and eosin (H&E) staining and Masson's trichrome (MT) staining.

2.5.2. Regeneration of Cranial Bone Defects

8-week-old male SD rats (230 ± 20 g, n = 3) were purchased from Chongqing Tengxinbier Laboratory Animal Sales Co., Ltd. and then divided into four groups, namely control (untreated), TCP, SSF1@TCP, SSF2@TCP, and SSF3@TCP. Animals were anesthetized using 3% pentobarbital sodium (30 mg kg^{-1}). Under sterile conditions, 5-mm diameter defects were made on the rats' skulls and defects were inserted with the scaffolds. By 8 weeks, rats were sacrificed by overdose of pentobarbital sodium (50 mg kg^{-1}), and specimens were harvested and fixed in 4% paraformaldehyde for micro-CT analysis and histological evaluation. In vivo bone regeneration at the defect site was analyzed on a micro-CT scanner (SkyScan 1176, Bruker). The 3D images of reconstructed bone tissues in the defect area were visualized using CTvox software. For histological analysis, specimens were decalcified in 10% ethylenediaminetetraacetic acid (EDTA) and embedded in paraffin. The specimens were sectioned (slice thickness, 4 mm) and stained with H&E and Masson's trichrome.

2.6. Statistical Analysis

All data were represented as mean ± standard error of the mean (SEM). Data was analyzed with GraphPad Prism Software v8.1 (San Diego, US). Significant differences were calculated with ANOVA single factor and P-value < 0.05 was considered statistically significant (*).

3. Results

3.1. Characterization of SSFx@TCP Cryogel Scaffolds

The fabrication process of cryogel scaffold is shown in Figure 1a. Silica fibers were first prepared through electrospinning and subsequently calcined to produce flexible silica fibers. These flexible silica fibers were then blended along with the TCP to afford crosslinked scaffolds. The calcination is a useful strategy for post-treatment to remove the organic components as well as enhance crystallinity and the thermal stability of SiO_2. As shown in **Figure** 2a, the pure SiO_2 fiber membrane exhibited optimal flexibility as revealed by the curling in the wet state alongside extensible recovery. Short SiO_2 fiber (SSF) powder obtained after homogenization showed a gray-black color (Figure 2d), with length and diameter values as 17.6 ± 10.9 µm (Figure 2f,j) and 0.32 ± 0.05 µm respectively (Figure 2i).

The crystallization temperature of SiO_2 is ca. 1200 °C.[16] It is therefore reasonable to expect that the SiO_2 can retain a part of its amorphous structure at calcination temperature lower than that of its crystallization temperature (approximately, 800 °C), which may impart flexibility characteristics alongside curling and bending while avoiding breaking upon exposure to the radial forces (Figure 1b). Consequently, the diameter of the calcined SiO_2 fibers was decreased (Figure 2b).[17] The short silica fibers (SSF) were homogeneously dispersed in an aqueous solution of the TCP (Figure 2c), the latter exhibited an average particle size of 0.78 ± 0.09 µm (Figure 2d,h) and was used as a reinforcing phase. Cryogel scaffolds were fabricated by molding, freeze-drying, and thermal crosslinking. Cryogel scaffolds maintained their structural integrity both in the dry as well as wet states (Figure 2e). The intensity of the diffraction peaks of the main crystalline phase (2θ, 30 °) was very high and sharp, which is suggestive of the successful incorporation of TCP particles alongside their good crystallinity (**Figure 3**d).[18]

The morphological analysis of cryogel scaffolds was carried out using SEM, which exhibited agglomerates of TCP particles on the uniformly distributed SSF (Figure 2g). EDS analysis manifested the presence of the elements, such as oxygen (O), silicon (Si), phosphorous (P), and calcium (Ca) elements on the surface of the scaffold, thereby further indicating the successful preparation of cryogel scaffolds (Figure 3b). X-ray photoelectron spectroscopy (XPS) showed peaks at 102 and 350 eV, which were ascribed to the Si 2p orbital Ca 2p orbital originating from silica nanofiber (Figure 3g).[19,20] For biomineralization, scaffolds were immersed in SBF for up to different time points. The content of the mineral components was increased with an increase in the incubation time (Figure 3c). The silanol (Si-OH) groups may furnish active sites for the biomineralization of the Ca and P.

With an increase in the amount of SSF, the density of the scaffolds was increased from 0.90 ± 0.12 mg cm^{-3} and 1.44 ± 0.21 mg cm^{-3} in SSF1@TCP and SSF2@TCP respectively to 1.80 ± 0.07 mg cm^{-3} in SSF3@TCP (Figure 2k), which was also in consistence with the water uptake of scaffolds (SSF1@TCP: 3830.70 ± 169.79%, SSF2@TCP: 4450.9 ± 144.8%, SSF3@TCP: 4553.7 ± 202.6%) (Figure 2l). Nevertheless, the volumetric shrinkage rate of the scaffolds in the wet state showed an opposite (e.g., SSF1@TCP, 22.10 ± 0.12% and SSF3@TCP, 12.43 ± 3.35%) (Figure 2m). These results suggested that the incorporation of SSF improved the stability of the scaffolds. Similarly, the mechanical properties of scaffolds were increased with an increase in the SSF content (Figure 3h). The uniaxial compressive strength (UCS) of SSF1@TCP was 3.03 ± 0.70 kPa, and SSF2@TCP was 3.35 ± 0.12 kPa, while that of the SSF3@TCP was 7.27 ± 0.59 kPa (Figure 3i). As compared to the SSF1@TCP, the SSF3@TCP exhibited 2.47 fold higher UCS. Similarly, the compression modulus of the scaffolds was increased from 2.67 ± 0.29 kPa in SSF1@TCP, to 3.05 ± 0.65 kPa in SSF2@TCP and 6.42 ± 0.55 kPa in SSF3@TCP (Figure 3j). The compression modulus of the SSF3@TCP was 3.16 fold higher than that

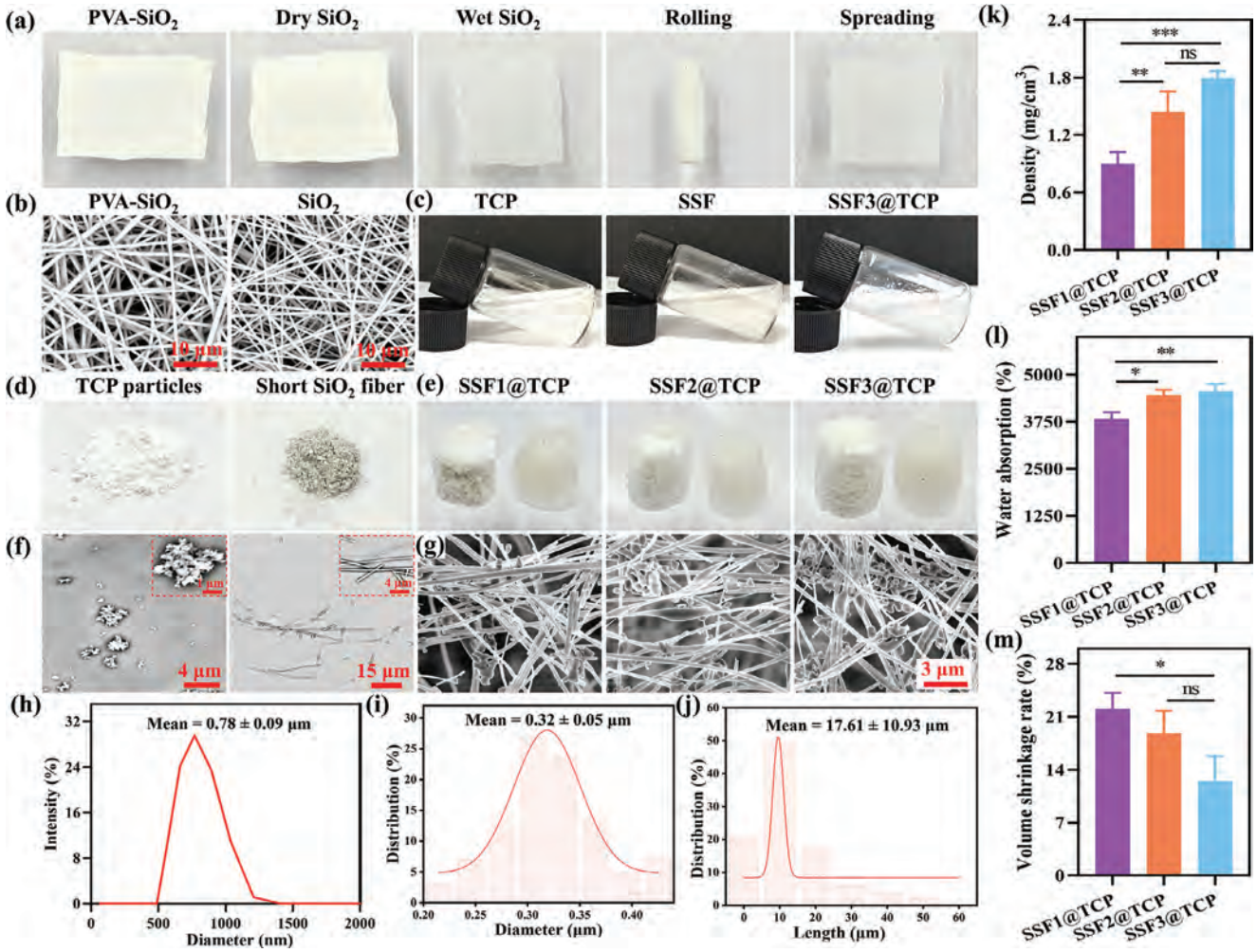

Figure 2. Morphological analysis of flexible SiO_2 membranes as well as cryogel scaffolds. a) Macroscopic images of PVA-SiO_2 fiber membrane and SiO_2 fiber membrane in dry and wet state. b) SEM image of PVA-SiO_2 fiber membrane and SiO_2 fiber membrane. c) Macroscopic images of TCP, SSF, and SSF3@TCP solution. d,e) Images of TCP particles, short SiO_2 fibers (SSF), and SSF1@TCP, SSF2@TCP, and SSF3@TCP scaffolds in the dry and wet state. f,g) SEM images of TCP particles, SSF, and SSF1@TCP, SSF2@TCP, and SSF3@TCP scaffolds. Diameter distribution of h) TCP particles, i) SSF, and length distribution of j) SSF. k) Density, l) water absorption, and m) volume shrinkage rate in wet state of SSF1@TCP, SSF2@TCP, and SSF3@TCP scaffolds. n = 3, $^{*}P < 0.05$, $^{**}P < 0.01$, and $^{***}P < 0.001$.

of the SSF1@TCP. These data manifested that the incorporation of SSF improved the mechanical properties of the scaffolds albeit lacking the necessary strength as well as the ability to endure the mechanical requirement of load-bearing bones (e.g., 0.1–2 GPa compression modulus of human cancellous bone and 7–20 GPa of cortical bone) in high-stress environments, thereby further limiting their widespread applications.[21] However, the increase in the amount of SSF did not significantly affect the pore size of the scaffolds, which were 3.25 ± 0.67, 3.44 ± 0.81, 3.72 ± 0.56 μm for SSF1@TCP, SSF2@TCP and SSF1@TCP, respectively (Figure S1, Supporting Information). This was consistent with the porosity results of the scaffolds and provided insight into great interconnectivity and homogeneity (SSF1@TCP: 84.01 ± 1.71%, SSF2@TCP: 85.30 ± 1.40%, SSF3@TCP: 85.52 ± 0.86%) (Figure S2, Supporting Information).

It is been well-proven that the therapeutic ions released from the scaffolds can promote vascularization as well as osteogenesis. Therefore we discerned the release kinetics of therapeutic ions released from scaffolds in vitro (Figure 3a).[22] Silicon ions (Si^{4+}) stimulate the proliferation and migration of vascular endothelial cells (ECs) and promote blood vessel formation as well as increase collagen production, structural integrity of the vascular wall, and strength and elasticity of blood vessels. Additionally, Si^{4+} may facilitate angiogenesis by regulating the expression of vascular endothelial growth factor (VEGF) and improve bone matrix synthesis, osteoblast proliferation, and mineralization.[23] On the other hand, calcium (Ca^{2+}) is the main mineral component of bone and is involved in the formation and mineralization of the bone matrix. Moreover, calcium ions (Ca^{2+}) play a key role in the activity of osteoblasts and contribute to bone repair and regeneration.[24] Phosphorus ions are an important component of bone, and along with calcium ions, they form HAp; the latter increases the hardness and stability of the bone. Moreover, phosphorus ions have been shown

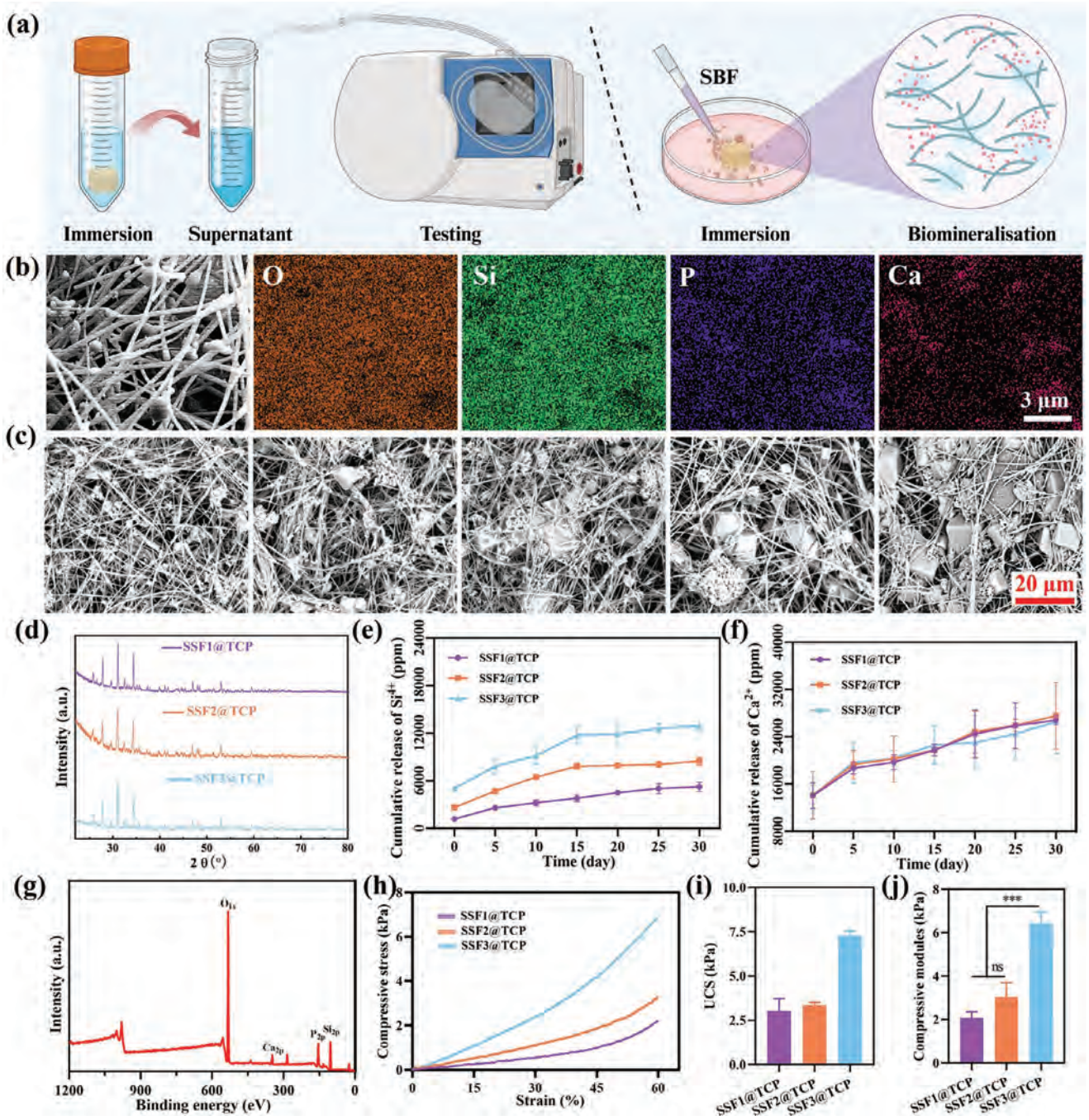

Figure 3. Physical characterization, biomineralization, and release of ions. a) Schematic diagram showing the procedure for the release of ions as well as biomineralization in vitro. b) EDS mapping of surface element distribution of SSF1@TCP scaffold. c) SEM image of the SSF3@TCP scaffold incubated in the SBF for 0, 5, 10, 20, and 30 days. d) XRD spectra of SSF1@TCP, SSF2@TCP, and SSF3@TCP scaffolds. The release of silicon ions Si^{4+} e) and calcium ions Ca^{2+} f) at different degradation time points. g) XPS spectrum of SSF3@TCP. h) Representative stress-strain curves, i) Uniaxial Compressive Strength (UCS), and j) compressive modules of SSF1@TCP, SSF2@TCP, and SSF3@TCP scaffolds. n = 3, $^{*}P < 0.05$, $^{**}P < 0.01$, and $^{***}P < 0.001$.

to enhance the proliferation and differentiation of osteoblasts as well as participate in bone repair.[25] The release of silicon ions (Si^{4+}) was consistent with the SSF content; the cumulative release of silicon ions (Si^{4+}) was found to be 6280.3 ± 795.9, 9920.7 ± 1541.4, and 12922.3 ± 566.5 ppm from the SSF1@TCP, SSF2@TCP, and SSF3@TCP scaffolds, respectively at day 30 (Figure 3e). The release kinetics of the other therapeutic ions, including calcium ions (Ca^{2+}) and phosphate ions (PO_4^{3-}) was also similar to that of the silicon ions (Si^{4+}) albeit the negligible difference among the different types of scaffolds partly due to the similar TCP content(Figure 3f; Figure S3, Supporting Information).

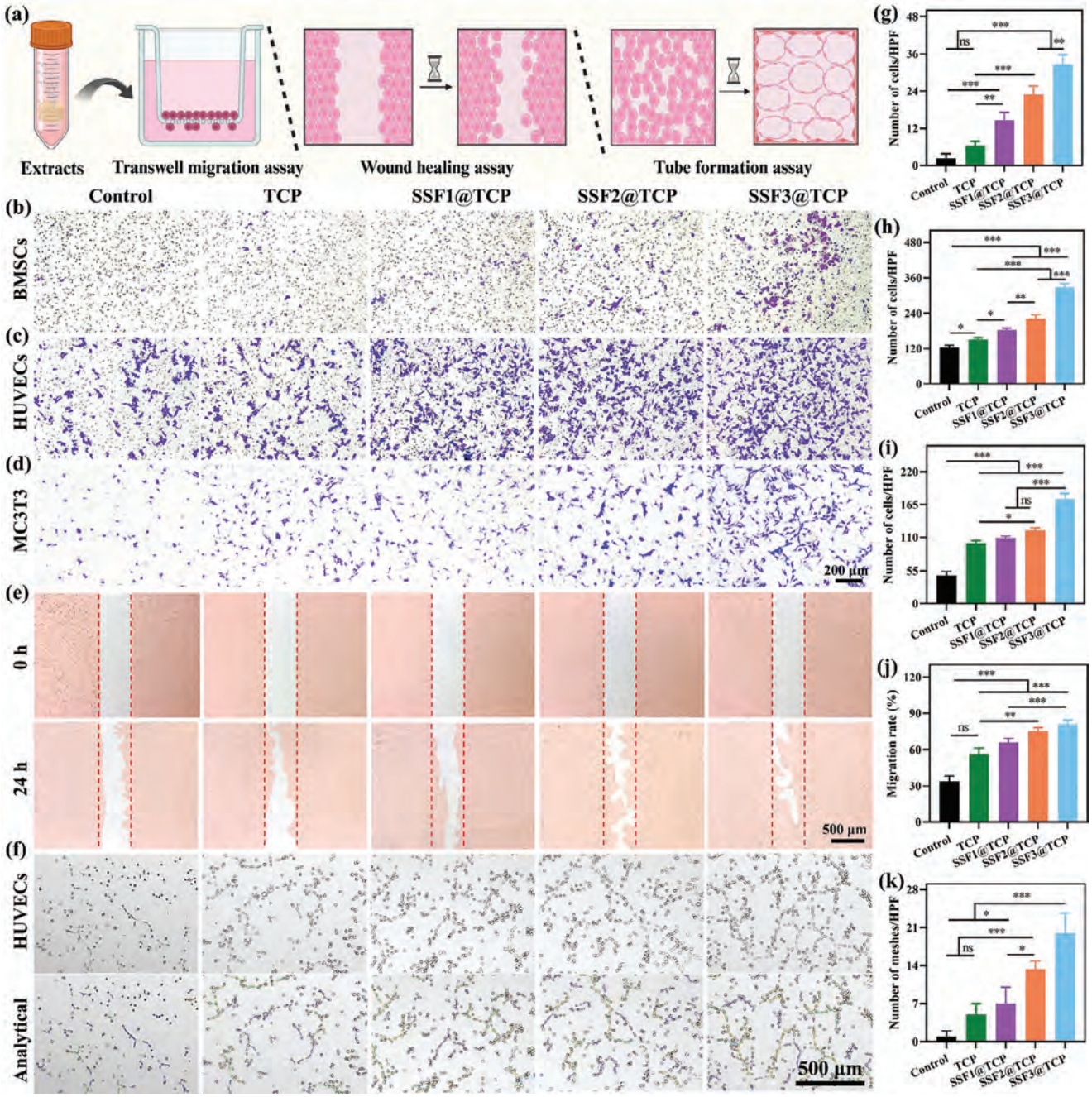

Figure 4. Transwell migration assay and scratch wounding assay using extract solution of different types of scaffolds. a) Schematic illustration of a Transwell migration assay, scratch wounding assay, and tube formation assay using the extract solution of different types of cryogel scaffolds in vitro. (b) Transwell migration assay using b) BMSCs, c) HUVECs, and d) MC3T3. e) Migration of HUCEVs in a scratch wounding assay. f) Tube formation assay of HUVECs for 6 h. Quantitative analysis of the number of migrated BMSCs g), HUVECs h), and MC3TC i), migration rate j), and the number of meshes k) in tube formation assay. n = 3, $^{*}P < 0.05$, $^{**}P < 0.01$, and $^{***}P < 0.001$.

3.2. Biocompatibility of SSFx@TCP Cryogel Scaffolds

The biological function of cryogel scaffolds in vitro was assessed using a Transwell migration assay, scratch wounding assay, and tube formation assay (**Figure** 4a). We delineated the migration of the MC3T3-E1 cell line and HUVECs. The MC3T3-E1 cell line is widely used to study bone formation and remodeling. Similarly, HUVECs are commonly used to study vascular biology, particularly angiogenesis and endothelial cell migration. Since bone is a highly vascularized tissue, it is important to study the migration of HUVEC in vitro (Figure 4c). In Transwell migration assay, we discerned the migration of HUVECs against the extract solution of the scaffolds containing varying content of SSF. The SSF3@TCP group outperformed all other groups in terms of the

number of cells migrated toward the lower side of the transwell inserts (SSF1@TCP, 183. 0 ± 5.6, SSF2@TCP, 222. 0 ± 13.4, SSF3@TCP, 327.3 ± 12.5, TCP, 150.7 ± 6.0, and control, 123.7 ± 7.5 per hpf) (Figure 4h). The migration of MC3T3 cells was also performed using a Transwell migration assay (Figure 4d). SSF3@TCP displayed 1.42, 1.59, 1.74, and 3.70 folds higher migration of MC3T3 cells than that of the SSF2@TCP, SSF1@TCP, TCP, and control groups, respectively (Figure 4i). Nonetheless, the chemotactic effect of the scaffold on the BMSCs was less pronounced (number of migrated BMSCs: SSF1@TCP, 14.7 ± 2.5, SSF2@TCP, 23.0 ± 2.7, SSF3@TCP, 32.7 ± 3.1, TCP, 6.3 ± 1.5, and control, 2.33 ± 1.53 per hpf) (Figure 4b,g). Improved migration of HUVECs and MC3T3 cells is ascribed to the ability of the scaffolds to furnish therapeutic ions, such as calcium ions (Ca^{2+}) and silicon ions (Si^{4+}), which promote the proliferation of HUVECs as well as induce angiogenic network formation.

In a scratch wounding assay using HUVECs, the wound closure rate was the most significant in the SSF3@TCP scaffolds than that of the other groups (SSF1@TCP, 33.7 ± 4.4%, SSF2@TCP, 75.40 ± 2.85%, SSF3@TCP, 80.8 ± 3.4%, TCP, 65.9 ± 3.5%, and control, 56.0 ± 5.3%) (Figure 4e,j).

Since angiogenesis plays a pivotal role in the vascularization of bone defects, we studied the ability of the scaffolds for the formation of tubule networks of HUVECs. SSF3@TCP group showed significantly higher angiogenic ability than that of the other groups (Figure 4f). Quantitative analysis revealed that the number of meshes was 20.0 ± 3.6 per hpf for the SSF3@TCP (Figure 4k). These results indicated that the silica-based cryogel scaffolds could significantly promote cell migration which may be ascribed to the release of silicon ions (Si^{4+}); the latter can inhibit the degradation of hypoxia-inducible factor 1-alpha (HIF-1α) by prolyl hydroxylase 2 (PHD2) and concurrently up-regulate the expression of HIF-1α. The HIF-1α can activate HIF-1α/VEGF/KDR/eNOS/NO and HIF-1α/FGF/FGFR signaling pathways to promote the recruitment, migration, proliferation and differentiation of cells.[25,26]

Since biomaterials often interact with the blood and can activate coagulation pathways, this necessitates the screening of biomaterials for hemocompatibility. Consequently, we discerned the hemocompatibility of cryogel scaffolds by performing hemolysis assay, activated partial thromboplastin assay (APTT), and blood clotting index (BCI) (**Figure 5**a). The supernatants in the SSF1@TCP, SSF2@TCP, and SSF3@TCP appeared to be lighter red than that of the positive control group (suspension of RBCs diluted with DI water), which is indicative of the negligible hemolysis by the scaffolds (Figure 5b). The hemolysis rate of all scaffolds was less than 2%, which meets the international standard (ISO 10993–4) (Figure 5f).[27] In a blood clotting assay, scaffolds, as well as medical gauze, were incubated along with the erythrocytes suspension (Figure 5c). While all groups led to blood coagulation, cryogel scaffolds manifested sluggish blood clotting (blood clotting time: SSF3@TCP, 105.0 ± 5.0, SSF2@TCP, 110.3 ± 3.2, SSF1@TCP, 115.7 ± 6.7 s, control, 190.0 ± 5.0 s) (Figure 5h).

Blood clotting assay in vitro was further leveraged to delineate the coagulation ability of scaffolds (Figure 5d). The RBCs were tightly adhered to the scaffolds, which remained intact even after washing with the water. The higher hemostatic ability of cryogel scaffolds may be ascribed to the release of calcium ions (Ca^{2+}), which have been shown to be involved in the coagulation cascade process. Moreover, calcium ions (Ca^{2+}) can also interact with the other blood clotting factors while acting on plasminogen, which cleaves fibrinogen and forms fibrin. Fibrin may then bind to platelets and RBCs to form a clot and prevent bleeding.[5] In contrast, RBCs could not be tightly adhered to the gauze and were mostly washed away with the water. The BCI values were quantified by measuring the absorbance of the suspension at 540 nm using a microplate reader. While SSF3@TCP and SSF2@TCP groups exhibited almost similar BCI, they exhibited significantly less BCI as compared to SSF1@TCP and gauze (BCI values: SSF3@TCP, 22.7 ± 1.5%, SSF2@TCP, 26.3 ± 0.8%, SSF1@TCP, 29.7 ± 0.9%),) gauze, 92.6 ± 3.4% (Figure 5g). Scaffolds were further evaluated by SEM to ascertain the adhesion of RBCs. As compared to SSF1@TCP and SSF2@TCP, the SSF3@TCP exhibited more numbers of adhered RBCs presumably due to an increase in the number of RBCs adhesion sites with an increase in the SSF content, thereby leading to higher blood clotting at a macroscopic level (Figure 5e). The silica-based materials have previously been shown to induce platelet activation. This process, marked by shape change, granule release, and surface receptor expression, is crucial for platelet aggregation and subsequent thrombus formation, thereby expediting hemostasis. The negatively charged surface of silica fibers at physiological pH facilitates electrostatic attraction with positively-charged ions, plasma proteins, and platelets, which can recruit and aggregate platelets, thereby enhancing blood coagulation.[28,29]

We next discerned the hemocompatibility of scaffolds using APTT assay and measured the associated parameters, including APTT, PT, and TT (Figure 5i–k). While SSF3 @TCP and SSF2@TCP almost similar APTT values, they were significantly less than that of the SSF1@TCP and gauze groups (APTT value: SSF3 @TCP, 31.0 ± 1.0, SSF2@TCP, 34.7 ± 1.5, SSF1@TCP, 38.0 ± 2.0, and gauze, 46.3 ± 1.5 s) (Figure 5i). Similarly, SSF2@TCP and SSF3@TCP exhibited almost similar PT values, these values were lower than that of the gauze (PT values: SSF3@TCP, 16.0 ± 1.0, SSF2@TCP, 15.0 ± 1.0, SSF1@TCP, 17.3 ± 1.5, and gauze, 20.0 ± 2.0 s)(Figure 5j). Moreover, the TT was appreciably less in the cryogel scaffolds than that of the gauze group (TT values: SSF3@TCP (10.0 ± 1.0, SSF2@TCP (11.0 ± 1.0, SSF1@TCP, 12.3 ± 0.6, and gauze, 13.3 ± 1.5 s) (Figure 5k). These results showed a better hemocompatibility of cryogel scaffolds than that of the gauze presumably due to the beneficial effect of the TCP, which may furnish calcium ions (Ca^{2+}); the latter is one of the members of the coagulation factors (IV). Silica fibers exhibit a high specific surface area, which may provide an invaluable platform for the adsorption of coagulation-related proteins, such as fibrinogen and von Willebrand factor (vWF).[30] This adsorption not only enhances the local protein concentration but also triggers conformational changes in the proteins that activate the coagulation cascade, particularly through an intrinsic pathway. Moreover, the negatively charged surface of silica fibers facilitates the activation of coagulation Factor XII (FXII) and initiates the intrinsic coagulation pathway.[31] Silica fibers may additionally leverage a structural matrix, which can support the polymerization and stabilization of fibrin fibers. This matrix may not only reinforce the physical

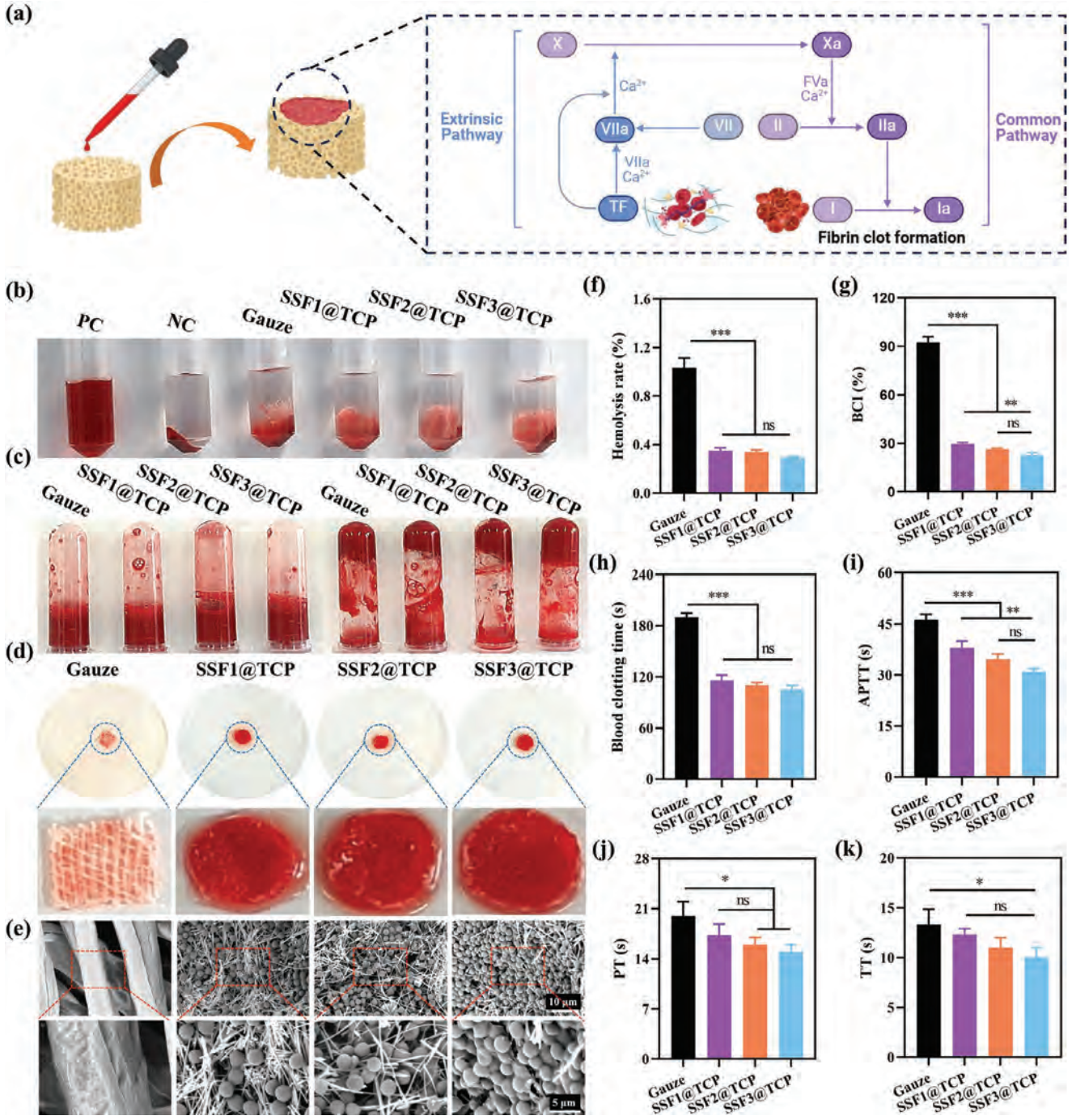

Figure 5. Hemocompatibility of cryogel scaffolds. a) Schematic illustration showing the extrinsic coagulation pathway for scaffold-mediated blood coagulation in vitro. b) Hemolytic activity and c) blood coagulation assay. d) Dynamic whole-blood clotting assay. e) SEM micrographs of red blood cells (RBCs) adhered to the scaffolds as well as gauze. Quantitative analysis of f) hemolysis rate, g) blood clotting index (BCI), h) blood clotting time, i) activated partial thromboplastin time (APTT), j) prothrombin time (PT), and k) thrombin time (TT). n = 3, $^{*}P < 0.05$, $^{**}P < 0.01$, and $^{***}P < 0.001$.

structure of the clot but it may also anchor the fibrin network, thereby increasing the resistance of the clot to the mechanical disruption.[32]

The cytocompatibility of scaffolds was further delineated in vitro using BMSCs and HUVECs and bioassay, including live/dead staining, CCK-8 assay, and cell cytoskeletal staining were carried out. Cells were cultured along with the extract solution of the different types of scaffolds. Both cell types displayed significant cell proliferation as evaluated for up to day 5. While all scaffolds were found to be cytocompatible, the SSF3@TCP scaffold significantly promoted cell proliferation (**Figure** 7b,e,f). The higher cell viability in the cryogel scaffolds, especially,

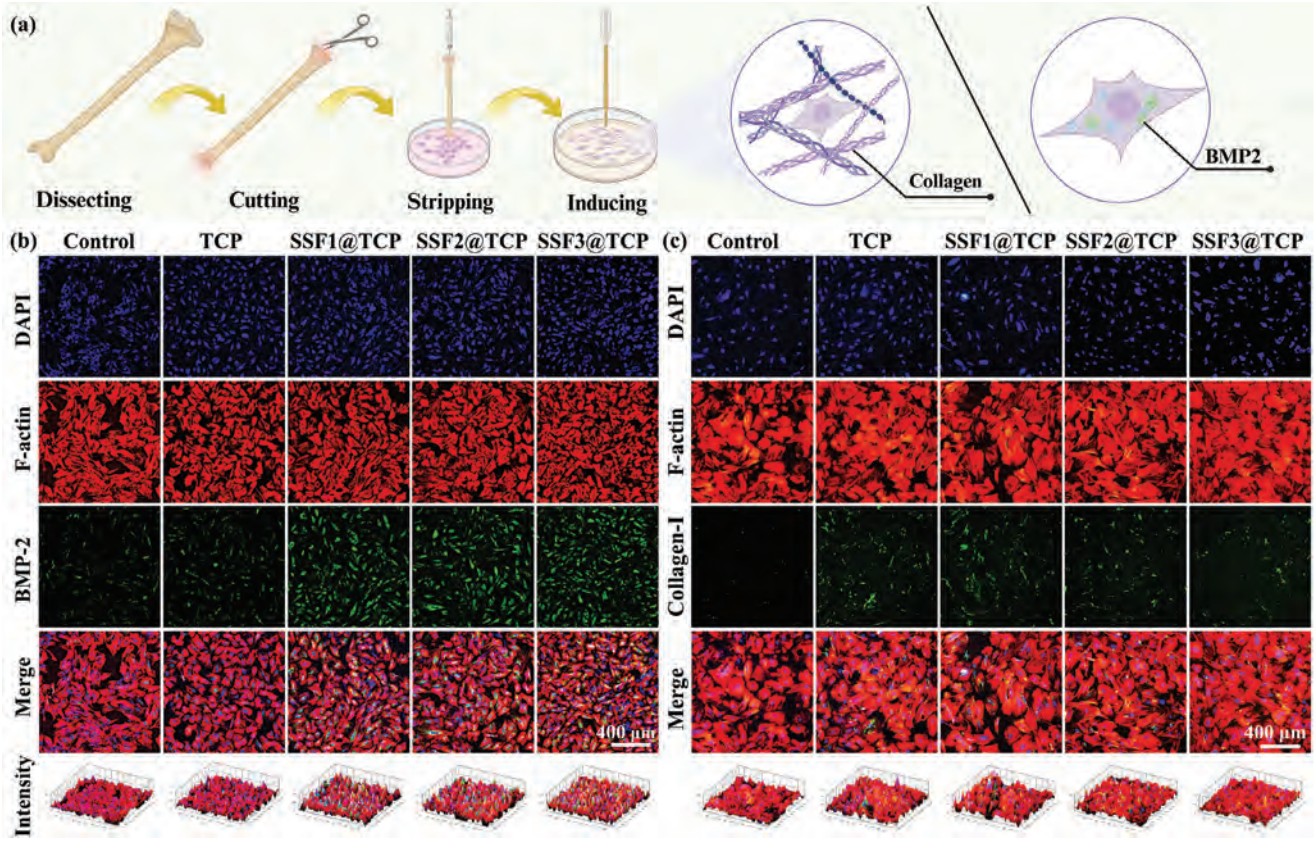

Figure 6. The osteogenic ability of scaffolds. a) Schematic illustration of the collection and induction of BMSCs to secrete collagen type I (Col-I) and bone morphogenetic protein 2 (BMP2). b) IF staining of the BMSCs cultured along with the extract solution of different scaffolds for up to 7 days. Cells were stained for the F actin, and BMP-2, while the nuclei were stained with the DAPI. c) IF staining of BMSCs for Col-I and F-actin. $^{*}P < 0.05$, $^{**}P < 0.01$, and $^{***}P < 0.001$.

SSF3@TCP may be ascribed to the synergistic effect of the silicon ions (Si^{4+}) and calcium ions (Ca^{2+}).[33] We additionally carried out cell cytoskeletal staining using cell-seeded constructs in vitro (Figure S4, Supporting Information), which manifested significant cell spreading in the SSF3@TCP scaffolds than that of the other groups. We anticipate that the scaffolds can furnish silicon ions (Si^{4+}), which may interact with the oxygen to form siloxane linkages; the latter may leverage metal-binding sites and thereby improve protein binding and stabilization both in the soluble form and with the scaffold. These siloxane linkages can introduce specific sites that can bind divalent cations, including calcium ions (Ca^{2+}) and magnesium ions (Mg^{2+}), and play a pivotal role in the stabilization of the secondary and tertiary structure of proteins. By binding these bivalent ions (e.g., Ca^{2+}, Mg^{2+}, etc.), the siloxane-rich surfaces may therefore effectively anchor proteins and enhance their stability and reduce denaturation. It is worth noting that silica and silicate materials have previously been shown to immobilize proteins and maintain their function.[33,34] The proteins adsorbed to the surface of the scaffold may interact with the cell surface integrins on BMSCs to mediate better cell adhesion.[9] It is worth noting that we cultured the cells on the scaffolds only for up to 3 days, which may be an insufficient time for appropriate cell adhesion, spreading, and growth.

3.3. Osteogenic Ability of Scaffolds

To delineate the osteogenic ability of scaffolds, BMSCs were cultured along with the extract solution of different types of scaffolds for up to day 7. Immunofluorescence (IF) staining was used to probe cell-secreted bone morphogenetic protein 2 (BMP2) and collagen type I (Col-I) alongside cell cytoskeleton staining to discern cell growth in vitro (**Figure 6a**). While all groups exhibited secreted F-actin, cryogels led to significantly higher production of F-actin than that of the TCP and control groups, which was further increased with an increase in the content of SSF in the scaffolds (Figure 6b). Similarly, Col-I production by the BMSCs was significantly higher in the cryogel groups as compared to the control group albeit slight reduction in the secretion of Col-I with an increase in the SSF content (Figure 6c). This decrease in the production of the Col-I with an increase in the SSF content may be ascribed to the fact that the lower concentrations of silicon ions (Si^{4+}) may promote collagen secretion, while the high concentration of the silicon ions (Si^{4+}) may suppress the production of Col-I.[35]

The ALP is widely recognized as an integral marker of osteogenic differentiation of BMSCs, which is upregulated during the earlier stages of osteogenesis (**Figure 7a**).[36] The ALP is expressed on the cell membrane of osteoblasts and is

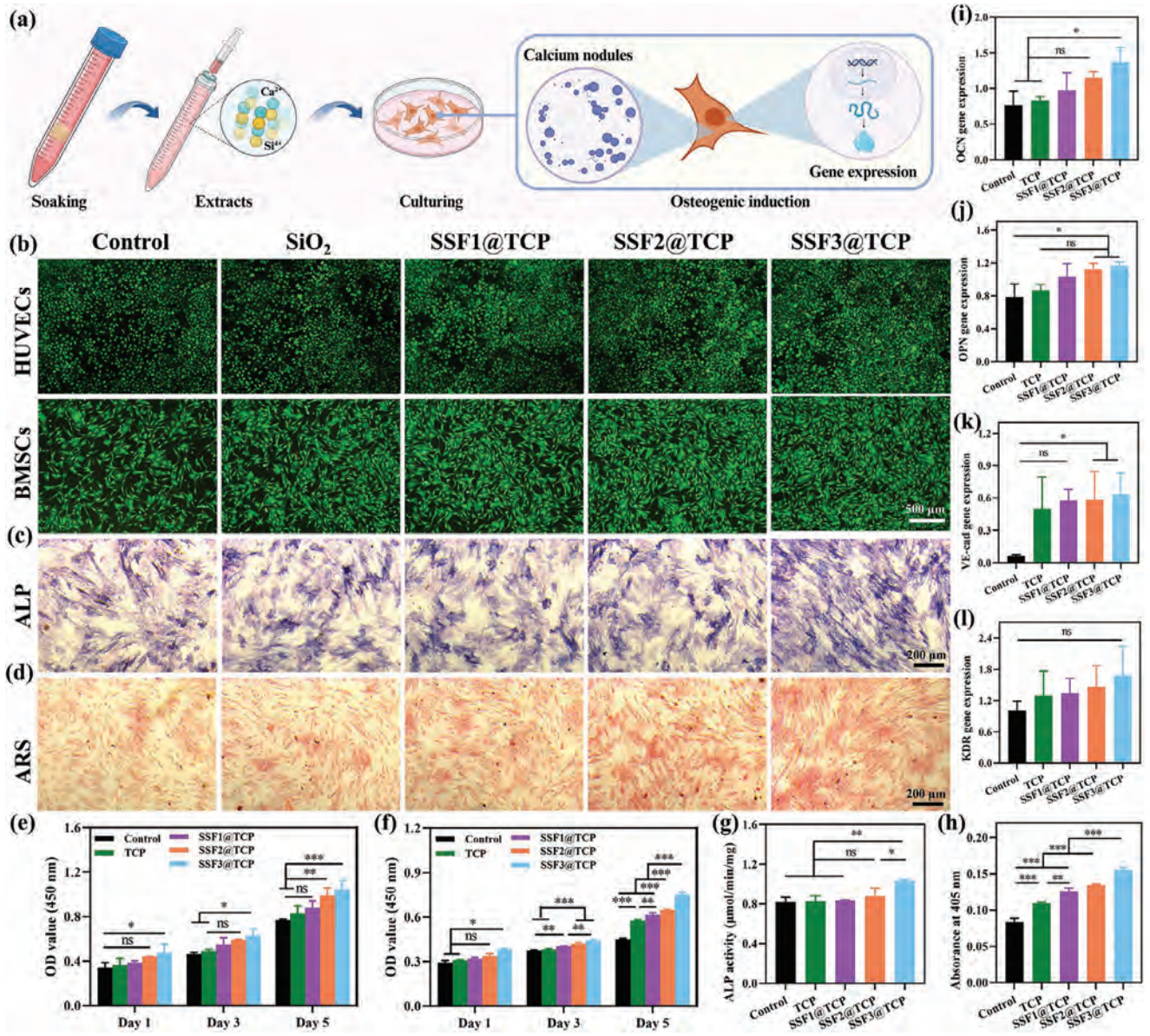

Figure 7. Osteogenic differentiation ability of the scaffolds. BMSCs were cultured along with the extract solution of the scaffolds for up to day 7. a) Schematic diagram of osteogenic differentiation induced by extract solution of different scaffolds. b) Live/dead staining. c) Microscopic images of ALP staining of BMSCs cultured with the conditioned medium from different scaffolds at day 7. d) Microscopic images of Alizarin Red S staining of BMSCs cultured with extracts from different scaffolds to observe the calcium nodule formation at day 7. e) HUVECs, f) BMSCs proliferation by CCK-8 assay at day 1, 3, and 5. g) Measurement of ALP activity at day 7. Quantitative analysis of ARS staining h), mRNA expression of gene OCN i), OPN j), VE-cad k), and KDR l). $^{*}P < 0.05$, $^{**}P < 0.01$, and $^{***}P < 0.001$.

discerned by ALP staining. On the other hand, the deposition is a marker of late-stage osteogenesis, which is revealed by the ARS staining. We therefore measured the ALP activity of BMSCs to delineate the osteogenic ability of the scaffolds at day 7. Both the SSF2@TCP and SSF3@TCP groups displayed significantly higher levels of ALP activity than that of the other groups, which is ascribed to the osteogenic stimulation of BMSCs by the release of therapeutic silicon ions (Si^{4+}) (Figure 7c,g). Similarly, ARS staining was performed, which displayed calcium nodules (see an intense red color) in all groups. Quantitative analysis exhibited a significantly higher number of calcium nodules in the cryogel scaffold groups (e.g., SSF1@TCP, SSF2@TCP, SSF3@TCP, etc.) as compared to the control and TCP; the SSF3@TCP group showed the highest number of calcium nodules (Figure 7d,h).

The osteogenic potential of the scaffolds was further probed by qPCR analysis. The expressions of osteogenic-related genes, including osteopontin (OPN) and osteocalcin (OCN) was detected once BMSCs were cultured along with the extract solution of various scaffolds for up to day 7. The mRNA levels of OPN and OCN were significantly higher in the cells cryogel scaffold groups (e.g., SSF1@TCP, SSF2@TCP, SSF3@TCP, etc.) than that of the

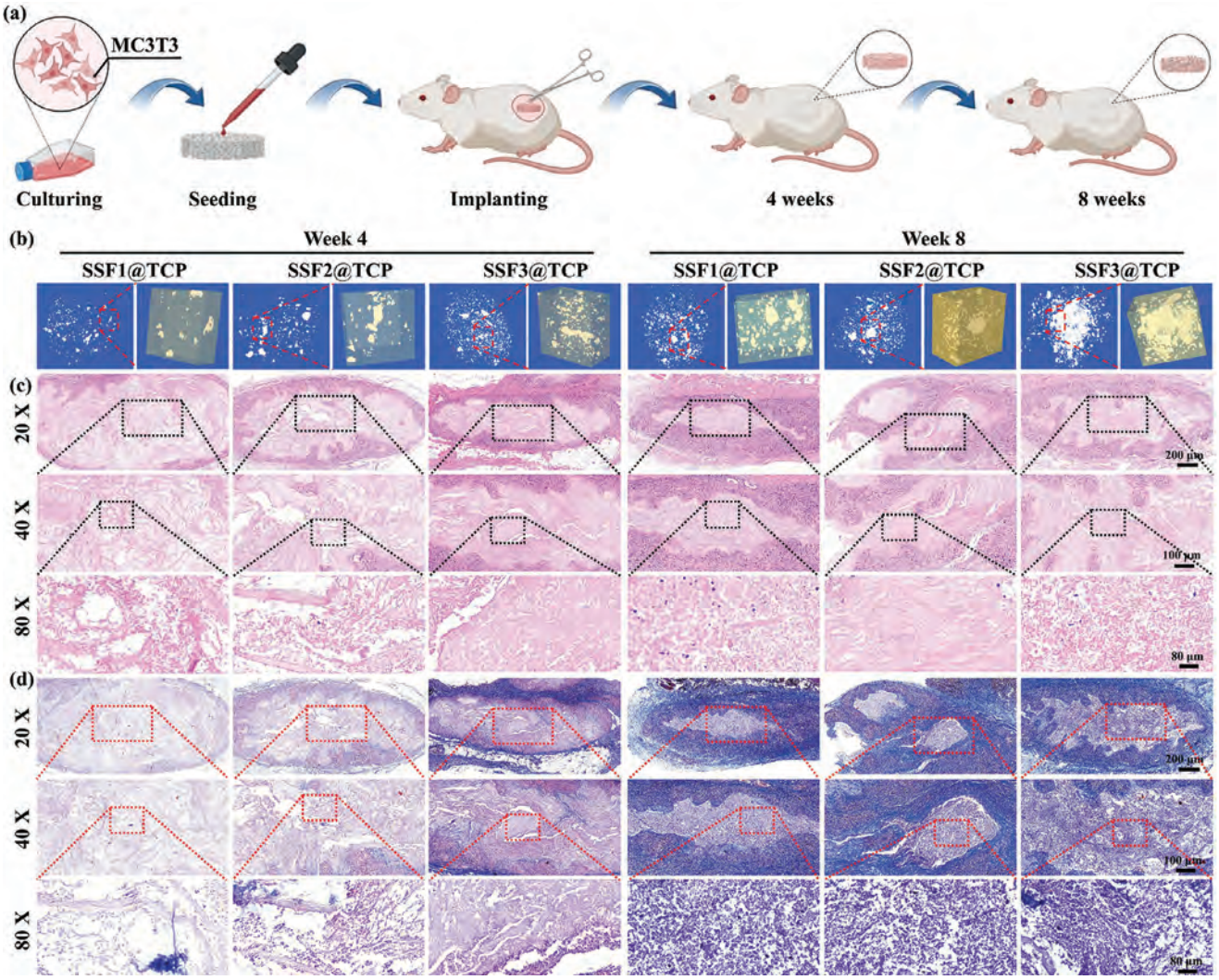

Figure 8. Ectopic bone formation assay. a) Schematic of implanting of MC3TC-loaded scaffolds. b) Micro-CT scanning after in vivo implantation for 4 and 8 weeks. c,d) Representative H&E and MT staining images after implanting for 4 and 8 weeks.

TCP and control groups. (Figure 7i,j). The SSF3@TCP scaffold displayed significantly higher mRNA expression of osteogenic-related genes presumably due to the large content of the SSF as compared to the other groups. Since bone is a vascularized tissue, we further employed qPCR to evaluate the expression levels of angiogenesis-related genes, including kinase insert domain receptor (KDR) and vascular endothelial cadherin (VE-cad) genes, The mRNA expression levels of the VE-cadherin gene were significantly higher than SSF2@TCP and SSF3@TCP in comparison to the other groups (Figure 7k), and there was no significant difference in the KDR expression levels among all groups may be due to the short cultivation time (Figure 7l). The higher osteogenic differentiation ability of the scaffolds is attributed to the release of therapeutic ions, such as calcium ions (Ca^{2+}) and silicon ions (Si^{4+}), which can synergistically act to promote osteogenesis and vascularization presumably through the MAPK signaling pathway. Calcium ions (Ca^{2+}) and silicon ions (Si^{4+}) have been shown to synergistically promote osteogenesis and angiogenesis, potentially through activation of the mitogen-activated protein kinase (MAPK) signaling pathway. Calcium ions (Ca^{2+}) play a pivotal role in inducing osteogenic differentiation by enhancing mineral deposition and stimulating the proliferation and differentiation of osteoblasts. Meanwhile, silicon ions (Si^{4+}) contribute to cellular signaling processes that promote vascularization, thereby supporting the migration and proliferation of HUVECs. Taken together, these ions can activate MAPK pathway components, such as ERK, JNK, and p38, which are known to regulate gene expression linked to osteogenic and angiogenic factors, thereby facilitating tissue regeneration and bone formation (Figure 1c).[37,38]

MC3T3 cells were first seeded in scaffolds and subsequently these MC3T3-seeded constructs were subcutaneously implanted in rats for up to 4 and 8 weeks (**Figure** 8a). The implanted scaffolds exhibited *de novo* bone-like tissues at 4 and 8 weeks, which is indicative of the osteogenic ability of scaffolds (Figure 8b,c). While most of the cells seeded in the middle region of the scaffolds were differentiated, undifferentiated MC-3T3E1 cells were mainly localized in the margins of the scaffolds at 4 weeks post-

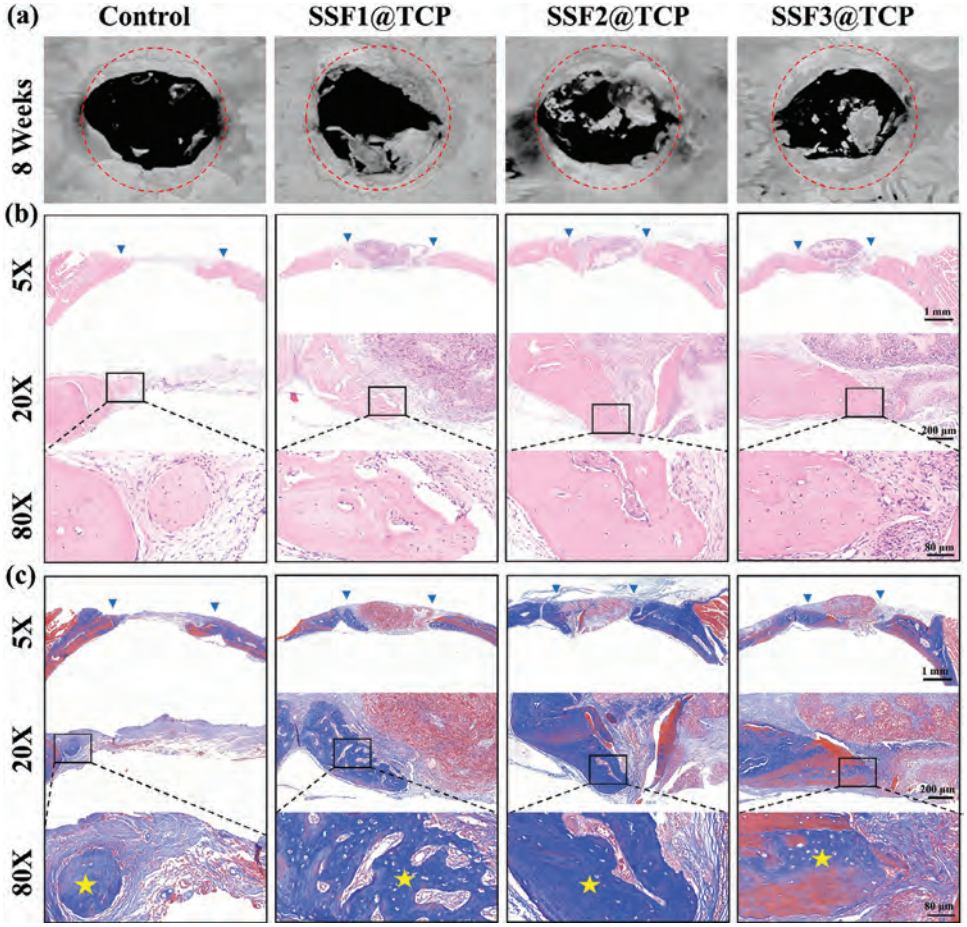

Figure 9. In vivo bone regeneration evaluation of different scaffolds in a rat calvarial defect model in rats. a) Representative 3D-reconstructed images after implantation of SSF1@TCP, SSF2@TCP, and SSF3@TCP scaffolds for 8 weeks. b,c) Histological analysis of calvarial bone sections at 8 weeks including H&E staining and Masson's trichrome staining.

transplantation. By week 8, the cell scaffold constructs exhibited a bone-like microstructure. Masson's trichrome staining manifested minute collagen deposition at the center region as early as week 4, which culminated into thick collagen deposits by week 8 post-transplantation (Figure 8d).

The pro-regenerative capacity of the scaffold was next discerned in a rat cranial defect model by week 8 post-transplantation (**Figure 9a**). The bone defect exhibited *de novo* bone tissues as revealed by the Micro-CT scanning. By week 8, the bone defect area was significantly decreased in all groups and was replaced with *de novo* bone tissues. It is worth noting that the bone defects transplanted with cryogel scaffolds (e.g., SSF1@TCP, SSF2@TCP, SSF3@TCP, etc.) displayed significantly higher formation of *de novo* bone tissues spanning from the interior of the defect toward its edges. In contrast, the control group (defect without scaffolds) possessed only marginal bone deposition within the defect area. The SSF3@TCP group outperformed the other groups both in terms of the neo-bone formation as well as the decrease in the defect area, which is ascribed to the synergistic effect of the SSF and TCP to induce *de novo* bone production and may also have implications for the application of these cryogel scaffolds for the fracture healing.[39]

The explanted scaffolds as well as bone tissues were further subjected to the histological analysis by the H&E staining and Masson's trichrome staining (Figure 9b,c). The control groups (defect without scaffolds) showed only a smaller portion of the regenerated bone tissues, which mainly occurred at the edge of the defect site. On the other hand, the defects treated with SSF2@TCP, and SSF3@TCP scaffold possessed more amount of regenerated bone tissues as compared to the SSF1@TCP (Figure 9a). We anticipate that this TCP portion of the scaffolds can slowly degrade and largely remain preserved, the portion of the scaffolds with the SSF can degrade rapidly to be replaced with the fibrous neo-bone tissues owing to its porous structure and fast degradation rate. Consequently, bone defects treated with the SSF2@TCP and SSF3@TCP were almost filled with mineralized bone tissue. The SSF3@TCP group exhibited a significant amount of the mineralized bone as well as the thickest bone matrix, which spanned not only the inner side of the defect but also the edges of the scaffolds. For an effective yet a healthy bone regeneration, the implanted scaffolds should degrade at a rate commensurate with the deposition of *de novo* bone tissues. Masson's trichrome staining manifested that the cryogel scaffolds were gradually absorbed and replaced with the collagenous

tissues (Figure 9c). Taken together, these data showed that the SSF3@TCP scaffold had an appropriate osteogenic ability and is capable of promoting bone defect repair, which may have implications for fracture healing for osteochondral defects.

4. Discussion

The bone is a connective, vascularized, and mineralized tissue, which confers protection to organs and participates in the support and locomotion of the human body, and maintenance of homeostasis, as well as in hematopoiesis. However, throughout the lifetime, bone defects may arise due to trauma (mechanical fractures), diseases, and/or aging, which may compromise the ability of the bone to self-regenerate. Consequently, bone-filling materials are widely used for bone tissue repair. The TCP mimics the inorganic components of the bone and has been extensively utilized as a bioresorbable ceramic for bone regeneration alongside its several merits, including good biocompatibility, low cytotoxicity, and minimal inflammatory responses in vivo.[40] Therapeutic ions released from the TCP could stimulate cell proliferation, differentiation, ECM production, and maturity in bone defect parts.[41]

However, several challenges hinder the applicability of the TCP for its successful utilization and clinical translation, such as poor vasculogenic ability, inferior mechanical strength, poor stability for storage and transportation, and weak integration with the host tissue. Moreover, the direct transplantation of the TCP may further lack a porous structure as often required for the scaffolds for bone tissue regeneration, tunable porosity and porous structure may enhance the diffusion of the oxygen and the transport of the nutrients throughout the scaffolds and facilitate vascularization. These limitations could be avoided by fabricating composite scaffolds with other components, including synthetic polymers and bioceramics fibers.[42,43]

An ideal scaffold for bone tissue engineering should have several basic characteristics: *i*) appropriate mechanical properties, *ii*) sufficient degradation as commensurate with the neo-tissue formation rate, *iii*) biocompatibility, *iv*) porosity for effective diffusion of oxygen as well as the transport of nutrients as well as accumulation of neo-tissues, and *v*) sustained and controlled release of therapeutics to actively steer cell proliferation and differentiation.[44] Short nanofiber-based cryogels, including PLLA/Gel fiber or SiO_2 fiber cryogels with high porosity, high water uptake, and appropriate mechanical properties have been extensively used for various application prospects, including skin repair, cartilage regeneration, and bone repair.[5,45]

Different polymers have been used to generate 3D cryogels. Synthetic polymers, such as PLLA and poly(lactic-co-glycolic acid) (PLGA), and poly (L-lactide-co-ε-caprolactone) (PLCL) are widely used to fabricate bone TE scaffolds, thanks to their ability to be fabricated into various shapes and structures as well as enable the sustained and controlled release of bioactive cues.[46] Despite the obvious advantages of these polymers, they lack cell recognition cues as well as osteo-inductive and osteo-conductive abilities. Since bioglass can furnish various therapeutic ions, including calcium ions (Ca^{2+}) and silicon ions (Si^{4+}), we prepared SiO_2 fiber to furnish silicon ions (Si^{4+}); the latter could improve cell migration and differentiation alongside enhancing the implant-host integration.[47,48] Consequently, to harness the synergistic benefits of the short SiO_2 fibers and TCP, we prepared 3D SSFx@TCP cryogel scaffolds.

In comparing SSFx@TCP scaffolds to commonly used bone repair materials, such as HAp-based composites and bioactive glass, several distinct advantages and challenges emerge in terms of bioactivity, mechanical strength, and degradation properties. HAp-based composites are highly osteoconductive, owing to their chemical similarity to natural bone, promoting osteoblast attachment and mineralization.[49] However, they are often limited by their relatively slow ion release rates and mechanical brittleness, which can impede their use in load-bearing applications. In contrast, bioactive glass (BG) exhibits a higher dissolution rate, enabling rapid ion release and enhanced osteogenic activity. This property makes BG highly effective for stimulating bone regeneration, but its fast degradation may lead to premature loss of mechanical integrity before the tissue is fully regenerated.[50] SSFx@TCP scaffolds, which combine the bioactive properties of both silica and TCP, provide a controlled release of calcium, phosphate, and silica ions, facilitating sustained osteogenesis and bone mineralization over a longer period. Compared to BG, SSFx@TCP scaffolds offer a more customizable degradation rate that aligns with the natural healing process, avoiding the rapid loss of scaffold integrity observed in bioactive glass. As compared to mesoporous silica nanoparticles (MSNs), SSFx@TCP scaffolds outperform these materials by providing both structural support and bioactivity, which is critical for large-scale bone TE applications. Furthermore, ion release from SSFx@TCP scaffolds is more controlled than that of other silica-based materials, thereby promoting bone regeneration through the sustained release of bioactive ions, including SiO_2, Ca^{2+}, and PO_4^{3-}, which have been shown to activate key signaling pathways like MAPK and Wnt/β-catenin, thereby enhancing osteoblast differentiation. However, further optimization of ion release kinetics and mechanical properties is necessary to fully realize their potential in clinical applications.

The SSFx@TCP scaffolds displayed a porous structure and good water uptake, which may be beneficial to promote cell infiltration from the host tissues in vivo. Since these composite cryogels can furnish the release of therapeutic ions, such as silicon ins (Si^{4+}) and calcium ions (Ca^{2+}), which can be further tailored by varying the composition of the SiO_2 fibers and TCP, they manifested good biomineralization. The mechanical properties of SSFx@TCP scaffolds, specifically their uniaxial compressive strength (UCS), are significantly lower than that of the mechanical strength required for most of the load-bearing bone applications. To address this challenge, several strategies can be explored to enhance the mechanical properties of SSFx@TCP scaffolds while preserving their bioactivity and porosity. One potential modification is the incorporation of secondary reinforcements, such as carbon nanofibers (CNFs), nanocellulose, and graphene oxide (GO), which are known for their excellent mechanical strength and biocompatibility. These materials can improve the compressive strength of the scaffolds without significantly reducing porosity or bioactivity, with CNFs and GO offering additional benefits like osteogenesis promotion and bone vascularization, respectively.[51,52] Another approach is crosslinking SSFx@TCP with bioactive polymers, such as collagen,[53] gelatin,[54] or polycaprolactone (PCL),[55] to enhance tensile strength and structural stability while maintaining bioactivity and supporting osteogen-

esis. However, it is important to carefully evaluate the trade-offs between mechanical strength and other critical scaffold properties, including porosity for cell infiltration and vascularization, as well as bioactivity, which may be impacted by the incorporation of reinforcing materials or crosslinking agents. In acknowledging the mechanical limitations of SSFx@TCP scaffolds, it is crucial to define their potential applications more clearly, recognizing that while the scaffolds may not be suitable for large, load-bearing bone defects, they could be highly effective for non-load-bearing applications, including craniofacial repairs, maxillofacial surgery, or small bone defects. Composite scaffolds incorporating SSFx@TCP could also be developed to meet the mechanical demands of more challenging clinical scenarios.

Composite cryogels also exhibited cytocompatibility presumably owing to the SiO_2 and TCP as evaluated using BMSCs and HUVECs. BMSCs show immuno-modulatory potential and can differentiate into bone-forming cells, such as osteoblasts, while HUVECs promote vascularization.[56] These scaffolds further enabled sustained release of calcium ions (Ca^{2+}) with negligible cytotoxicity.

Bone repair involves the combined effect of different cell types to precisely regulate osteoblastic, osteoclastic, and angiogenic activities. The SSF3@TCP scaffolds showed higher cell migration in a scratch wounding assay as well as a transwell migration assay in vitro. Enhanced wound repair may partly be ascribed to the release of therapeutic ions, such as silicon ions (Si^{4+}); the latter can upregulate the expression of hypoxia-inducible factor-1α (HIF1-α), vascular endothelial growth factor-A (VEGFA), and vascular endothelial growth factor receptor-2 (VEGFR-2) and promote vascularization for bone defect repair. Moreover, silicon ions (Si^{4+}) could promote cell-cell interaction and cell growth, and can additionally reduce cell apoptosis due to an exaggerated oxidative environment at the defect site.[57] The porous architecture of SSFx@TCP scaffolds makes them particularly suitable for defects requiring high vascularization, such as critical-sized cranial bone defects or long bone non-load-bearing scenarios. These scaffolds excel in promoting vascular EC migration and tubule formation, key for vascularized bone regeneration. In our work, we measured the pore size of the scaffolds using SEM in combination with the gravimetry method. While this method may not accuratley measure the pore size of the scaffolds, it may provide an insight into an overall void fraction, which correlates with the pore architecture. The potential of scaffolds may however be limited, especially, in load-bearing applications due to relatively lower compressive strength as compared to the cortical bone, thereby necessitating further reinforcement or hybridization with the incorporation of additional reinforcing agents, such as ceramic particles (e.g., HAp, BG, etc.). We can also alter the polymer matrix by incorporating cross-linking agents to improve rigidity and durability. In addition, optimization of processing conditions may also be a potential solution for the better control of porosity and density.

Since bone is a highly vascularized tissue, bone fracture may damage vasculature and lead to bleeding, thereby constricting bone tissue repair. In an in vitro coagulation assay, SSFx@TCP scaffolds promoted blood coagulation as revealed by the high BCI values and reduced blood clotting time, PT, and APTT. The efficient blood clotting can be due to different types of factors. First, cryogels displayed a hollow structure and exhibited significant water absorption properties, which can absorb spilled blood. Thereafter, TCP and SiO_2 fiber may release Ca^{2+} and Si^{4+} to activate intrinsic and extrinsic coagulation pathways, as well as promote the phosphorylation of platelet protein by protein kinase C (PKC), to activate the blood coagulation cascade, thereby facilitating blood clot formation to prevent bleeding.[14]

Bone healing involves a coordinated interaction of different types of cells.[58] The SSFx@TCP scaffolds exhibit significant osteogenic ability in vitro as revealed by the ALP and ARS assays alongside significant osteogenic promotion effect in an ectopic bone formation assay. In a rat calvarial defect model, composite scaffolds promoted bone repair, which may be ascribed to the synergistic effect of SSF and TCP components alongside 3D porous structure. It has been previously shown that Si-based biomaterials can release Si^{4+} and Ca^{2+}, which could stimulate biomineralization, enhance osteoblast differentiation, and improve collagen type I (Col-I) deposition.[13,59] Second, Si^{4+} and Ca^{2+} released from the SSFx@TCP scaffolds upregulated the expression of osteogenic and angiogenesis-related genes (e.g., OCN, OPN, VE-cad, KDR, etc.), as well as improved the production of the BMP-2 and Col-I, which may further promote bone repair by simultaneously inducing angiogenesis and osteogenesis. Thirdly, the implanted biomaterial surface architecture such as nano/microstructure surface could act on the attachment and spread of relative cells to affect cytokine and chemokine secretion to facilitate osteogenesis and osteointegration, thereby further promoting bone regeneration.[60]

Together, the aerogels could create a favorable microenvironment to trigger several biological events, such as the recruitment of BMSCs, secretion of angiogenesis and osteogenesis factors, and promotion of osteoclastogenesis, which accelerated bone formation and material resorption coupling to achieve bone healing. Therefore, these aerogels exerted the inherent properties of TCP and SiO_2 while leveraging advancements in nanoparticle electrospinning, and functionalization to develop diverse functionalities and resolve present technological challenges, which promote the versatility of biomaterials.

5. Conclusion

We prepared composite cryogels containing SSF and TCP using electrospinning combined with freeze-drying. Tissue-engineered scaffolds prepared by silica fibers and TCP exhibit ECM-mimetic structure and high bioactivity characteristics, which may alleviate the problems of conventional bioceramics, which are dense, brittle, and fragile. These composite scaffolds promoted bone healing by absorbing spilled blood rapidly (blood clotting time: 105.0 ± 5.0 s), enabling the sustained release of bioactive ions (6280.3 ± 795.9 ppm of Si^{4+} at day 30), thereby facilitating mineral deposition, enhancing vascularization, and stimulating the activity of BMSCs. Our evaluations revealed good biocompatibility and pronounced osteogenic potential, while the calvarial defect model assay demonstrated significant enhancements in bone regeneration in vivo. These cryogel scaffolds may release therapeutic ions, such as Ca^{2+} and Si^{4+} may synergistically promote angiogenesis as well as osteogenesis via an up-regulation of the expression of the HIF-1α and MAPK signaling pathways. Collectively, these findings underscore the potential of these scaffolds as an innovative solution for wound repair, and bone defects. This mate-

rial may serve as a valuable resource for investigating novel approaches in bone tissue engineering.

Supporting Information

Supporting Information is available from the Wiley Online Library or from the author.

Acknowledgements

X.W., Z.Y. and G.C. contributed equally to this work. This project was supported by the Science and Technology Research Program of Chongqing Municipal Education Commission (Grant No. KJZD-K202412807), Youth Doctoral Talent Incubation Program of the Second Affiliated Hospital, Army Medical University (2023YQB002), Science and Technology Commission of Shanghai Municipality, China (20DZ2254900, 21DZ2222300), Sino German Science Foundation Research Exchange Center, China (M-0263), and China Education Association for International Exchange (2022181). This project was also supported by the Chenguang Program of Shanghai Education Development Foundation and Shanghai Municipal Education Commission (23CGB08), Researchers Supporting Project Number (RSP2025R65), King Saud University, Riyadh, Saudi Arabia. Thanks to http://www.home-for-researchers.com for assistance with the creation of Figure 1.

Conflict of Interest

The authors declare no conflict of interest

Data Availability Statement

The data that support the findings of this study are available on request from the corresponding author. The data are not publicly available due to privacy or ethical restrictions.

Keywords

bone regeneration, cryogel, electrospinning, short silica nanofiber, tricalcium phosphate

Received: November 4, 2024
Revised: February 3, 2025
Published online:

[1] A. Nauth, E. Schemitsch, B. Norris, Z. Nollin, J. T. Watson, *J. Orthop. Trauma* **2018**, *32*, S7.
[2] J. Zhang, B. Zhang, Z. Zheng, Q. Cai, J. Wang, Q. Shu, L. Wang, *Adv. Funct. Mater.* **2022**, *32*, 2109882.
[3] M. Zhang, R. Lin, X. Wang, J. Xue, C. Deng, C. Feng, H. Zhuang, J. Ma, C. Qin, L. Wan, J. Chang, C. Wu, *Sci. Adv.* **2020**, *6*, eaaz6725.
[4] X. Zhou, Y. Qian, L. Chen, T. Li, X. Sun, X. Ma, J. Wang, C. He, *ACS Nano* **2023**, *17*, 5140.
[5] X. Wang, Z. Yuan, M. Shafiq, G. Cai, Z. Lei, Y. Lu, X. Guan, R. Hashim, M. El-Newehy, M. M. Abdulhameed, X. Lu, Y. Xu, X. Mo, *ACS Appl. Mater. Interfaces* **2024**, *16*, 25843.
[6] P. Dhavalikar, D. Jenkins, N. Rosen, A. Kannapiran, K. Salhadar, O. Shachaf, M. Silverstein, E. Cosgriff-Hernández, *J. Mater. Chem. B* **2023**, *11*, 10651.
[7] Z. Yuan, L. Zhang, S. Jiang, M. Shafiq, Y. Cai, Y. Chen, J. Song, X. Yu, H. Ijima, Y. Xu, X. Mo, *Smart Mater. Med.* **2023**, *4*, 407.
[8] Z. Yuan, L. Zhang, H. Zheng, M. Shafiq, J. Song, *J. Drug Deli. Sci. Technol.* **2023**, *89*, 105072.
[9] M. Liu, X. Wang, J. Cui, H. Wang, B. Sun, J. Zhang, B. Rolauffs, M. Shafiq, X. Mo, Z. Zhu, J. Wu, *J. Mater. Chem. B* **2023**, *11*, 359.
[10] F. Monte, T. Cebe, D. Ripperger, F. Ighani, H. V. Kojouharov, B. M. Chen, H. K. W. Kim, P. B. Aswath, V. G. Varanasi, *J. Tissue Eng. Regen. Med.* **2018**, *12*, 2203.
[11] A. E. Stoica (Oprea), A. C. Bîrcă, O. Gherasim, A. Ficai, A. M. Grumezescu, O.-C. Oprea, B. Ştefan Vasile, C. Balta, E. Andronescu, A. O. Hermenean, *Pharmaceutics* **2023**, *15*, 1728.
[12] Z. Yuan, L. Zhang, H. Zheng, M. Shafiq, J. Song, B. Sun, M. EL-Newehy, H. EL-Hamshary, Y. Morsi, C. Huang, X. Mo, Y. Xu, *J. Drug Deli. Sci. Technol.* **2023**, *89*, 105072.
[13] X. Wang, Z. Yuan, M. Shafiq, G. Cai, Z. Lei, Y. Lu, X. Guan, R. Hashim, M. El-Newehy, M. M. Abdulhameed, X. Lu, Y. Xu, X. Mo, *ACS Appl. Mater. Interfaces* **2024**, *16*, 25843.
[14] Q. Hou, K. Liu, C. Lian, J. Liu, W. Wei, T. Qiu, H. Dai, *Biomacromolecules* **2023**, *24*, 3397.
[15] Z. Chen, C. Wu, W. Gu, T. Klein, R. Crawford, Y. Xiao, *Biomaterials* **2014**, *35*, 1507.
[16] L. Wang, Y. Qiu, H. Lv, Y. Si, L. Liu, Q. Zhang, J. Cao, J. Yu, X. Li, B. Ding, *Adv. Funct. Mater.* **2019**, *29*, 1901407.
[17] X. Song, W. Liu, S. Xu, J. Wang, B. Liu, Q. Cai, S. Tang, Y. Ma, *J. Eur. Ceram. Soc.* **2018**, *38*, 201.
[18] M. Isik, J. D. Avila, A. Bandyopadhyay, *Addit. Manuf.* **2020**, *36*, 101553.
[19] F. Akti, S. Balci, *Mater. Chem. Phys.* **2023**, *297*, 127347.
[20] A. C. Özarslan, C. Özel, S. Yücel, Y. B. Elalmis, *Ceram. Int.* **2024**, *50*, 30980.
[21] A. Kashirina, Y. Yao, Y. Liu, J. Leng, *Biomater. Sci.* **2019**, *7*, 3961.
[22] S. Majumdar, A. Tiwari, D. Mallick, D. K. Patel, S. K. Trigun, S. Krishnamurthy, *ACS Omega* **2024**, *9*, 7188.
[23] M. Liu, M. Shafiq, B. Sun, J. Wu, W. Wang, M. EL-Newehy, H. EL-Hamshary, Y. Morsi, O. Ali, A. U. R. Khan, X. Mo, *Adv. Healthcare Mater.* **2022**, *11*, 2200499.
[24] P. Wei, J. Zhou, S. Xiong, F. Yi, K. Xu, M. Liu, H. Xi, Z. Zhou, Z. Qiu, H. Liu, J. Zeng, Y. Liu, P. Qiu, J. Zhou, S. Liu, Z. Long, J. Li, L. Xiong, *ACS Appl. Mater. Interfaces* **2024**, *16*, 9768.
[25] G. Cai, Z. Yuan, X. Wang, S. Wu, S. Zhou, Z. Lei, P. Li, M. EL-Newehy, M. Moydeen Abdulhameed, M. Shafiq, X. Mo, S. Jiang, H. Gu, *Chem. Eng. J.* **2024**, *500*, 156555.
[26] K. Dashnyam, G.-Z. Jin, J.-H. Kim, R. Perez, J.-H. Jang, H.-W. Kim, *Biomaterials* **2017**, *116*, 145.
[27] X. Zhang, X. Zhang, B. Du, X. Wang, X. Ruan, W. Zheng, Y. Dai, M. Guo, G. He, *J. Membr. Sci.* **2024**, *690*, 122183.
[28] B. Li, H. Tang, X. Bian, K. Ma, J. Chang, X. Fu, C. Zhang, *Burns & Trauma* **2021**, *9*, tkab029.
[29] T. Chen, Z. Zhang, D. Weng, L. Lu, X. Wang, M. Xing, H. Qiu, M. Zhao, L. Shen, Y. Zhou, J. Chang, H.-P. Li, *Bioact. Mater.* **2021**, *6*, 3194.
[30] A. T. Bauer, E. A. Strozyk, C. Gorzelanny, C. Westerhausen, A. Desch, M. F. Schneider, S. W. Schneider, *Biomaterials* **2011**, *32*, 8385.
[31] M. Heestermans, C. Naudin, R. K. Mailer, S. Konrath, K. Klaetschke, A. Jämsä, M. Frye, C. Deppermann, G. Pula, P. Kuta, M. A. Friese, M. Gelderblom, A. Sickmann, R. J. S. Preston, J.-R. Nofer, S. Rose-John, L. M. Butler, O. Salomon, E. X. Stavrou, T. Renné, *Nat. Commun.* **2021**, *12*, 5596.
[32] N. A. Arce, W. Cao, A. K. Brown, E. R. Legan, M. S. Wilson, E.-R. Xu, M. C. Berndt, J. Emsley, X. F. Zhang, R. Li, *Nat. Commun.* **2021**, *12*, 2360.
[33] R. Majeed, H. M. Elnawawy, M. G. Kutty, N. A. Yahya, N. H. Azami, N. H. Abu Kasim, M. S. Nabhan, P. R. Cooper, J. Camilleri, H. M. A. Ahmed, *Odontology* **2023**, *111*, 759.

[34] L. S. Connell, L. Gabrielli, O. Mahony, L. Russo, L. Cipolla, J. R. Jones, *Polym. Chem.* **2017**, *8*, 1095.
[35] P. Uribe, A. Johansson, R. Jugdaohsingh, J. J. Powell, C. Magnusson, M. Davila, A. Westerlund, M. Ransjö, *Sci. Rep.* **2020**, *10*, 9923.
[36] A. K. Gaharwar, S. M. Mihaila, A. Swami, A. Patel, S. Sant, R. L. Reis, A. P. Marques, M. E. Gomes, A. Khademhosseini, *Adv. Mater.* **2023**, *35*, 2300774.
[37] P. Zhou, D. Xia, Z. Ni, T. Ou, Y. Wang, H. Zhang, L. Mao, K. Lin, S. Xu, J. Liu, *Bioact. Mater.* **2021**, *6*, 810.
[38] R. A. Youness, D. M. Tag El-deen, M. A. Taha, *Silicon* **2023**, *15*, 2493.
[39] M. K. Yadav, V. Pandey, K. Mohanta, V. K. Singh, *Ceram. Int.* **2022**, *48*, 25335.
[40] H. Lin, S. Shi, X. Lan, X. Quan, Q. Xu, G. Yao, J. Liu, X. Shuai, C. Wang, X. Li, M. Yu, *Small Methods* **2021**, *5*, 2100536.
[41] T. Kageyama, H. Akieda, Y. Sonoyama, K. Sato, H. Yoshikawa, H. Isono, M. Hirota, H. Kitajima, Y.-S. Chun, S. Maruo, J. Fukuda, *Acta Biomater.* **2023**, *165*, 168.
[42] L. B. C. Cavalcanti, H. P. A. Alves, S. C. Santos, K. G. Spaniol, E. A. dos Santos, W. Acchar, *Ceram. Int.* **2023**, *49*, 31576.
[43] S. V. Lopes, M. N. Collins, R. L. Reis, J. M. Oliveira, J. Silva-Correia, *ACS Appl. Bio. Mater.* **2021**, *4*, 2941.
[44] S. P. Malliappan, A. A. Yetisgin, S. B. Sahin, E. Demir, S. Cetinel, *Carbohydr. Polym.* **2022**, *283*, 119142.
[45] L. Qin, G. Jing, N. Cui, Z. Xu, Y. He, Y. Qin, T. Lu, J. Sun, A. Du, S. Wang, *Adv. Compos. Hybrid Mater.* **2022**, *6*, 3.
[46] P. Song, D. Zhou, F. Wang, G. Li, L. Bai, J. Su, *Mater. Today Bio.* **2024**, *29*, 101296.
[47] V. Uskoković, G. Abuna, J. R. Hampton, S. Geraldeli, *Pharmaceutics* **2024**, *16*, 39.
[48] B. Karakuzu-Ikizler, P. Terzioğlu, Y. Basaran-Elalmis, B. S. Tekerek, S. Yücel, *Bioact. Mater.* **2020**, *5*, 66.
[49] X. Gui, B. Zhang, Y. Qin, H. Lei, X. Xia, Y. Li, H. Lei, X. Zhou, Y. Tan, Z. Dong, Q. You, C. Zhou, Y. Fan, *Composites, Part A* **2025**, *189*, 108600.
[50] Q. Lei, Y. Chen, S. Gao, J. Li, L. Xiao, H. Huang, Q. Zhang, T. Zhang, F. Yan, L. Cai, *Mater. Des.* **2023**, *227*, 111754.
[51] H. Derakhshankhah, H. Nekounam, Z. Izadi, Z. Allahyari, M. Samari, M. feizi, H. Samadian, *J. Drug Deliv. Sci. Technol.* **2023**, *89*, 105082.
[52] M. E. Berrio, A. Oñate, A. Salas, K. Fernández, M. F. Meléndrez, *Mater. Today Chem.* **2021**, *20*, 100422.
[53] R. Li, S. Xu, Y. Guo, C. Cao, J. Xu, L. Hao, S. Luo, X. Chen, Y. Du, Y. Li, Y. Xie, W. Gao, J. Li, B. Xu, *J. Orthop. Transl.* **2025**, *50*, 129.
[54] H. Zhu, H. J. Haugen, G. Perale, J. Elin Reseland, L. Parreiras Nogueira, A. Gonzalez Cantalapiedra, F. Maria Guzon Muñoz, M. Permuy Mendaña, F. Betge, S. Petter Lyngstadaas, J. Xiao, *Engineering* **2022**, *13*, 197.
[55] R. Liu, Y. Pang, T. Xiao, S. Zhang, Y. Liu, Y. Min, *Int. J. Biol. Macromol.* **2022**, *218*, 1.
[56] S. Lian, Z. Mu, Z. Yuan, M. Shafiq, X. Mo, W. Mu, *Regen. Biomater.* **2024**, *11*, rbae022.
[57] K. Awad, N. Ahuja, M. Fiedler, S. Peper, Z. Wang, P. Aswath, M. Brotto, V. Varanasi, *Int. J. Mol. Sci.* **2021**, *22*, 497.
[58] H. Peng, T. Ling, Y. Zhang, T. Xie, X. Pei, K. Zhou, A. Chen, J. Chen, X. Zhu, X. Zhang, Z. Zhou, *ACS Appl. Mater. Interfaces* **2023**, *15*, 9120.
[59] F. Monte, T. Cebe, D. Ripperger, F. Ighani, H. V. Kojouharov, B. M. Chen, H. K. W. Kim, P. B. Aswath, V. G. Varanasi, *J. Tissue Eng. Regener. Med.* **2018**, *12*, 2203.
[60] N. Xu, J. Fu, L. Zhao, P. K. Chu, K. Huo, *Adv. Healthcare Mater.* **2020**, *9*, 2000681.

